magnetochemistry

MDPI

Communication

Two One-Dimensional Copper-Oxalate Frameworks with the Jahn–Teller Effect: $[(CH_3)_3NH]_2[Cu(\mu\text{-}C_2O_4)(C_2O_4)]\cdot 2.5H_2O$ (I) and $[(C_2H_5)_3NH]_2[Cu(\mu\text{-}C_2O_4)(C_2O_4)]\cdot H_2O$ (II)

Bin Zhang [1,*], Yan Zhang [2], Zheming Wang [3,*], Yang Sun [4], Tongling Liang [4], Mei Liu [4] and Daoben Zhu [1,*]

1 Organic Solid Laboratory, BNLMS, CMS & Institute of Chemistry, Chinese Academy of Sciences, Beijing 100190, China
2 Department of Physics, Institute of Condensed Material Physics, Peking University, Beijing 100871, China; zhang_yan@pku.edu.cn
3 State Key Laboratory of Rare Earth Materials Chemistry and Applications, BNLMS, College of Chemistry and Molecular Engineering, Peking University, Beijing 100871, China
4 BNLMS, CMS & Institute of Chemistry, Chinese Academy of Sciences, Beijing 100190, China
* Correspondence: zhangbin@iccas.ac.cn (B.Z.); zmw@pku.edu.cn (Z.W.); zhudb@iccas.ac.cn (D.Z.)

Abstract: Two one-dimensional oxalate-bridged Cu(II) ammonium salts, $[(CH_3)_3NH]_2[Cu(\mu\text{-}C_2O_4)(C_2O_4)]\cdot 2.5H_2O$ (**I**) and $[(C_2H_5)_3NH]_2[Cu(\mu\text{-}C_2O_4)(C_2O_4)]\cdot H_2O$ (**II**) were obtained and characterized. They were composed of ammonium: $(CH_3)_3NH^+$ in (**I**), $(C_2H_5)_3NH^+$ in (**II**), $[Cu(\mu\text{-}C_2O_4)(C_2O_4)^{2-}]_n$ and H_2O. The Jahn–Teller-distorted Cu(II) is octahedrally coordinated by six O atoms from three oxalates and forms a one-dimensional zigzag chain. The hydrogen bonds between ammonium, the anion and H_2O form a three-dimensional network. There is no hydrogen bond between the anion chains. They were insulated at 20 °C with a relative humidity of 40%. Ferromagnetic and weak-ferromagnetic behaviors were observed in **I** and **II**, separately. No long-range ordering was observed above 2 K.

Keywords: Jahn–Teller effect; Cu(II); oxalate; crystal structure; conductivity; magnetism

Citation: Zhang, B.; Zhang, Y.; Wang, Z.; Sun, Y.; Liang, T.; Liu, M.; Zhu, D. Two One-Dimensional Copper-Oxalate Frameworks with the Jahn–Teller Effect: $[(CH_3)_3NH]_2[Cu(\mu\text{-}C_2O_4)(C_2O_4)]\cdot 2.5H_2O$ (I) and $[(C_2H_5)_3NH]_2[Cu(\mu\text{-}C_2O_4)(C_2O_4)]\cdot H_2O$(II). *Magnetochemistry* **2023**, *9*, 120. https://doi.org/10.3390/magnetochemistry9050120

Academic Editor: Carlos J. Gómez García

Received: 20 March 2023
Revised: 27 April 2023
Accepted: 27 April 2023
Published: 29 April 2023

1. Introduction

The Jahn–Teller effect plays an important role in inorganic superconductors and colossal magneto-resistance materials [1–9]. Interesting conductivity and magnetic behaviors are expected when the Jahn–Teller effect exists in molecular crystals, such as metal–organic frameworks. Oxalate ($C_2O_4^{2-}$), as one of the most commonly used short connectors, plays a key role in molecular-based magnets [10–12]. Long-range ordering has been reported in metal–oxalate framework compounds from one-dimensional zigzag chains ($K_2Fe(\mu\text{-}C_2O_4)(C_2O_4)$, $K_2Co(\mu\text{-}C_2O_4)(C_2O_4)$, $Co(\mu\text{-}C_2O_4)(\mu\text{-}HOC_3H_6OH)$, $TTF[Fe(\mu\text{-}C_2O_4)Cl_2]$ and κ-$BETS_2[Fe(\mu\text{-}C_2O_4)Cl_2]$) to two-dimensional honeycomb lattices ($[(C_4H_9)_4N][CrMn(\mu\text{-}C_2O_4)_3]$, $A[M^{II}Fe^{III}(\mu\text{-}C_2O_4)_3]$ (A = ammonium; M = Mn, Fe), $[C_5H_{10}N_3O]_2[Fe_2(\mu\text{-}C_2O_4)_3]$, $Fe_2(\mu\text{-}C_2O_4)_3\cdot 4H_2O$) and square lattices ($[Fe(\mu\text{-}C_2O_4)(CH_3OH)]_n$) to three-dimensional metal–oxalate framework compounds ($[Co(bpy)_3][Co_2(\mu\text{-}C_2O_4)_3]ClO_4$, $Mn(\mu\text{-}C_2O_4)(H_2O)_{0.25}$, $[Z^{II}(bpy)_3][M^{II}Cr^{III}(\mu\text{-}C_2O_4)_3][ClO_4]$ (M = Mn, Fe, Co, Ni) and $(Me_4N)_6[Mn_3Cr_4(\mu\text{-}C_2O_4)_{12}]\cdot 6H_2O$), while a single chain magnet $[C_{12}H_{24}O_6K]_{0.5}[(C_{12}H_{24}O_6)(FC_6H_4NH_3)]_{0.5}[Co(H_2O)_2Cr(\mu\text{-}C_2O_4)(C_2O_4)_2]$ has been reported [13–29].

Quantum spin liquid is an intriguing magnetic state, where spin ordering or freezing prevents spin frustration in a resonating valence bond (RVB) state. In 1979, P. W. Anderson proposed the RVB state in $S = 1/2$, a two-dimensional triangular lattice [30]. In 1987, he proposed that La_2CuO_4 is a parent compound of cuprate superconductors. The

antiferromagnetic insulator La_2CuO_4 turns into a diamagnetic superconductor after hole doping, and a quantum spin liquid with Jahn–Teller distortion on Cu(II) is an indispensable magnetic state [31]. The spin-frustrated copper-oxalate framework with Jahn–Teller distortion supports a platform for molecular-based quantum spin liquids [32,33]. Strong antiferromagnetic interactions without a long-range ordering above 2 K with spin frustration were observed in two-dimensional honeycomb lattices: θ^{21}-(BEDT-TTF)$_3$[Cu$_2$(μ-C$_2$O$_4$)$_3$]·2CH$_3$OH, θ^{21}-(BETS-TTF)$_3$[Cu$_2$(μ-C$_2$O$_4$)$_3$]·2CH$_3$OH, [(C$_3$H$_7$)$_3$NH]$_2$[Cu$_2$(μ-C$_2$O$_4$)$_3$]·2.2H$_2$O, hydrogen-bonded square lattice β″-(BEDT-TTF)$_3$[Cu$_2$(μ-C$_2$O$_4$)(C$_2$O$_4$)$_2$(CH$_3$OH)(H$_2$O)], and three-dimensional hyperhoneycomb lattice [(C$_2$H$_5$)$_3$NH]$_2$[Cu$_2$(μ-C$_2$O$_4$)$_3$] [34–38]. [(C$_2$H$_5$)$_3$NH]$_2$[Cu$_2$(μ-C$_2$O$_4$)$_3$], which is a quantum spin liquid with no long-range ordering was observed until 60 mK [39]. In these compounds, the antiferromagnetic behavior depends on the antiferromagnetic interaction between the ferromagnetic couple. The magnetic structure of [(C$_2$H$_5$)$_3$NH]$_2$[Cu$_2$(μ-C$_2$O$_4$)$_3$] is lower than the three-dimensional, with the coexistence of ferromagnetic and antiferromagnetic interactions between Jahn–Teller distorted Cu(II) [37,39]. Researching the magnetic properties of Jahn–Teller distorted one-dimensional copper-oxalate frameworks [Cu(μ-C$_2$O$_4$)(C$_2$O$_4$)$_2^{2-}$]$_n$ without the hydrogen bond between anions will help us to quantitatively analyze the magnetic interaction in Jahn–Teller-distorted two-dimensional and three-dimensional copper-oxalate frameworks and design new candidate quantum spin liquids. Two one-dimensional copper-oxalate framework compounds, [(CH$_3$)$_3$NH]$_2$[Cu(μ-C$_2$O$_4$)(C$_2$O$_4$)]·2.5H$_2$O (**I**) and [(C$_2$H$_5$)$_3$NH]$_2$[Cu(μ-C$_2$O$_4$)(C$_2$O$_4$)]·H$_2$O (**II**), have been obtained and characterized. The related work is presented here.

2. Experiment

[(CH$_3$)$_3$NH]$_2$[Cu(μ-C$_2$O$_4$)(C$_2$O$_4$)]·2.5H$_2$O (**I**) and [(C$_2$H$_5$)$_3$NH]$_2$[Cu(μ-C$_2$O$_4$)(C$_2$O$_4$)]·H$_2$O (**II**) were obtained from a methanol solution of Cu(NO$_3$)$_2$·3H$_2$O and H$_2$C$_2$O$_4$·2H$_2$O with (CH$_3$)$_3$N for **I** and (C$_2$H$_5$)$_3$N for **II** in a 1:3:5 ratio at room temperature. Bulk blue plateful crystals of **I** and **II** were obtained after four weeks. The crystal was washed with CH$_3$COOC$_2$H$_5$ and dried. Elemental analysis calculated (%) for C$_{10}$H$_{25}$CuN$_2$O$_{10.50}$ (**I**): C 29.67, H 6.22 and N 6.92 and found C 29.87, H, 6.08 and N 6.97. For C$_{16}$H$_{34}$CuN$_2$O$_9$ (**II**): C 41.60, H 7.42, N 6.06 and found C 42.03, H 7.46 and N 6.11.

Elemental analyses of carbon, hydrogen and nitrogen were performed using the Flash EA 1112 elemental analyzer. The IR spectra were recorded on a Bio-rad FTS6000/UMA500 spectrometer (Figure S1). Thermogravimeter analysis was carried out on a Shimadzu DTG-60 analyzer at a 10 °C/min heating rate from room temperature to 550 °C under N_2 gas with an Al bag. **I** remains stable until 40 °C, and **II** remains stable until 80 °C.

X-ray powder diffraction was carried out using a Rigaku RINT2000 diffractometer at room temperature with Cu Kα radiation (λ = 1.54056 Å) in a flat-plate geometry (Figures S2 and S3).

Single-crystal X-ray diffraction was carried out on an Enraf-Nonius KappaCCD diffractometer at room temperature. The crystal structure was solved using the direct method and refined using the full-matrix least square on F^2 using the SHELX program, with anisotropic thermal parameters for all non-hydrogen atoms [40]. The hydrogen atoms on C and N were located through calculation, and on H_2O they were located through a difference Fourier map. All of the H were refined isotropically. The crystallographic data are listed in Table S1.

The resistance measurement was performed on a single crystal at Tonghui TH2828. Gold wires were attached to the best developed surfaces of a single crystal with a size of 0.40 ∗ 0.30 ∗ 0.11 mm (**I**) and 0.71 ∗ 0.60 ∗ 0.17 mm (**II**) using gold paste. The two-probe conductivity was measured at 20 °C and a relative humidity (RH) of 40%.

Magnetization measurements were performed on a polycrystalline sample tightly packed into a capsule on a Quantum Design MPMS 7XL SQUID system above 2 K. Susceptibility data were corrected for the diamagnetism of the sample by Pascal constants

and background by experimental measurement of the sample holder [41]. Temperature-dependent magnetization was performed under an applied field of 1000 G. Isothermal magnetization was measured at 2 K from 0 to 65 kG.

3. Result and Discussion

I crystallizes in a triclinic system with space group $P\ \bar{1}$. There are two $(CH_3)_3NH^+$, one Cu^{2+}, one oxalate anion, two half-oxalate anions and one-and-a-half H_2O coexisting in an independent unit (Figure 1). Cu^{2+} is coordinated to two O atoms from one bidentate oxalate (O1 and O2) and four O atoms from two disbidentate oxalates in the Q_3 Jahn–Teller distortion mode of a CuO_6 octahedron [8].

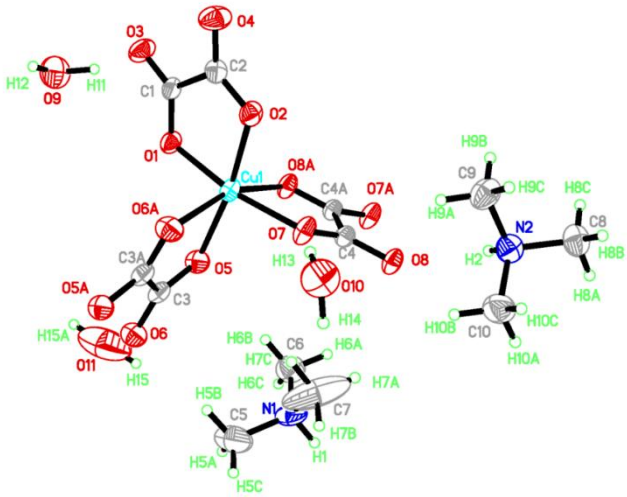

Figure 1. Atomic structure of **I** in an independent unit with scheme label and 50% ellipsoids. Asymmetry code for C3A, O5A, O6A: 2 − x, 2 − y, −z; C4A, O7A, O8A: 1 − x, 1 − y, −z; H15A: −x, 2−y, −z.

The Cu–O distances are 1.954(2)~1.992(2) Å on the equatorial plane and 2.292(2) Å, 2.329(2) Å from the apex as a result of the Jahn–Teller distortion. The elongated Cu–O bonds (Cu1–O6, Cu1–O8) on the Jahn–Teller-distorted octahedron around Cu^{2+} are highlighted with solid black lines (Figure 2). The cis O–Cu–O angles are 77.73° and 77.12° for the bridged oxalate, 83.56° for the terminal oxalate, and 90.70°, 98.89°, 90.31°, 96.85°, 93.12° and 100.68° among the terminal and bridged oxalate. The trans O–Cu–O angles are in the range of 161.01(6)~171.46(6)°. The axial Cu to oxalate-oxygen angles are 109.17° (Cu1–O6–C3) and 108.27° (Cu1–O8–C4). A one-dimensional zigzag $[Cu(\mu\text{-}C_2O_4)(C_2O_4)^{2-}]_n$ is formed along the *b* axis.

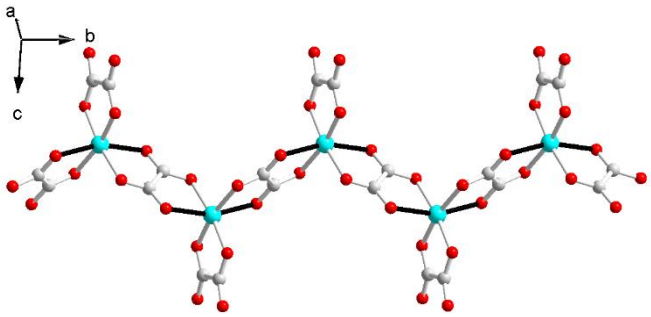

Figure 2. The zigzag anionic chain in **I**.

The one-dimensional $[Cu(\mu\text{-}C_2O_4)(C_2O_4)^{2-}]_n$ zigzag chain running along the *b* axis is separated by $(CH_3)_3NH^+$ (N1) along the *c* axis, and there are hydrogen bonds N–H···O, C–

H···O between the cation and the out O atom in the oxalate. The anionic sheets composed of a $[Cu(\mu\text{-}C_2O_4)(C_2O_4)^{2-}]_n$ chain and $(CH_3)_3NH^+$ in a 1:1 ratio are separated by a cation layer composed of a zigzag $(CH_3)_3NH^+$ (N2) chain and a zigzag H_2O chain along the *c* axis. There are hydrogen bonds between neighboring H_2O molecules. Five H_2O molecules formed a hydrogen-bond $[H_2O]_5$ linear cluster along the *c* axis (Figure 3).

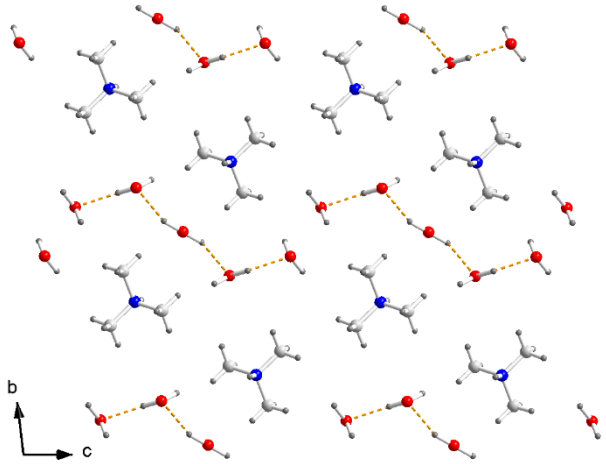

Figure 3. Arrangement of $(CH_3)_3NH^+$ and H_2O in cation layer of **I**. Dashed yellow lines are hydrogen bonds between H_2O in $[H_2O]_5$.

At last, the hydrogen bonds N–H···O and C–H···O between the ammonium and the inner O of the terminal and bridged oxalate, the O–H···O between H_2O and the oxalate, and the O–H···O between the H_2O molecules form a three-dimensional hydrogen-bonded network in crystal (Figure 4). There is no hydrogen bond between the anions.

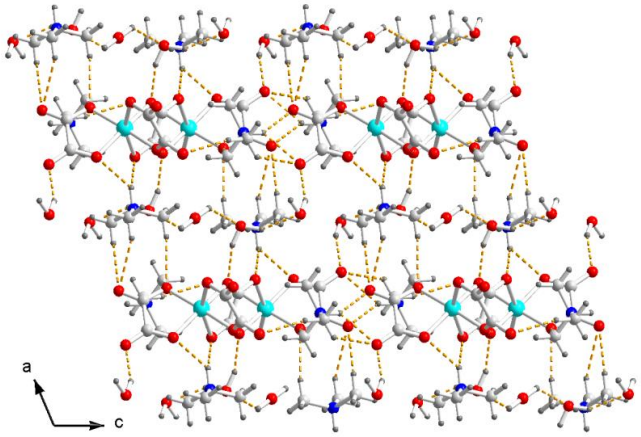

Figure 4. Packing diagram of **I** viewed along the *b* axis. Dash yellow lines are hydrogen bonds. Color code: Cu, cyan; O, red; C, white; N, blue; H, light grey.

II crystallizes in a monoclinic system with the space group $P2_1/c$. There are two $(C_2H_5)_3NH^+$, one Cu^{2+}, one and two half oxalates, and one H_2O in an independent unit (Figure 5). The Cu^{2+} is octahedrally coordinated by six O atoms from two bisbidentate oxalates and one bidentate oxalate, as in **I**, with Cu–O distances of 1.960(2)~1.999(2) Å on the equatorial plane, and Cu1–O8: 2.314(2) Å and Cu1–O7: 2.368(2) Å from the apex. The Cu–O distances of **II** in the equatorial plane are shorter than the direction of the apex as a result of the Q_3 Jahn–Teller distortion mode, as in **I**. The cis–O–Cu–O angles are 75.93° and 77.79° for the bridged oxalate, 88.31° for the terminal oxalate and 92.34°, 93.72°, 95.98°,

89.66°, 95.48° and 102.48° between the terminal and bridged oxalate. The trans-O–Cu–O angles are in the range of 160.21(7)~172.64(7)°. The axial Cu to oxalate-oxygen angles are 108.09° (Cu1–O1–C3) and 108.53° (Cu1–O8–C4). The Cu–O distances and O–Cu–O angles in **I** and **II** are in the same range of the Cu–oxalate coordination polymer [29,30,34,35,37,38]. A one-dimensional oxalate-bridged zigzag $[Cu(\mu\text{-}C_2O_4)(C_2O_4)^{2-}]_n$ chain is formed along the *b* axis.

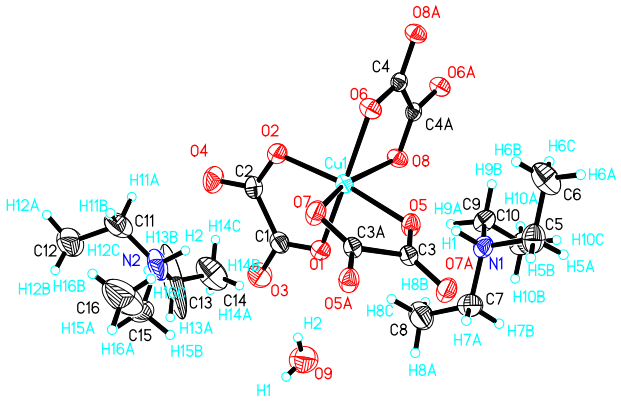

Figure 5. ORTEP drawing of **II** in an independent unit with scheme label and 50% ellipsoids. Asymmetry code for C3A, O5, O7: −x, −y, 1 − z; C4A, C6A, C8A: −x, 1−y, 1 − z.

The zigzag chain in **I** and **II** is centrosymmetric with the inversion center located at the middle point of the oxalate bridge; thus, the metal sites have a ΔΛΔΛ configuration along the *b* axis in **I** and **II** (Figure 6). It is similar to $[(CH_3)_4N]_2Cu(C_2O_4)_2(H_2O)$ [42,43]. The hydrogen bonds between ammonium and the anion and H_2O and the anion influence the bond length of the CuO_6 octahedron due to the Jahn–Teller distortion. Due to the magnetic orbitals of $dx^2 - y^2$ on Cu(II) with the unpaired electrons parallel to each other and the axial Cu to oxalate-oxygen angles, which are sensitive to magnetic interaction and smaller than 109.5°, a ferromagnetic interaction was expected [43,44].

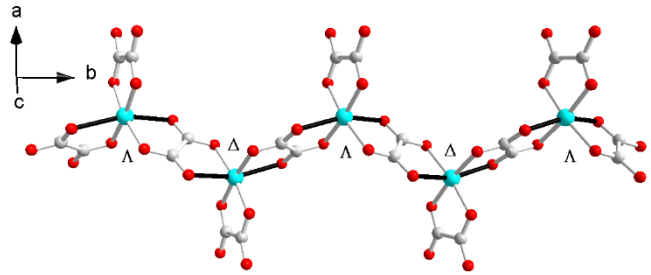

Figure 6. The zigzag anionic chain in **II**.

In **II**, the $[Cu(\mu\text{-}C_2O_4)(C_2O_4)^{2-}]_n$ chain is surrounded by zigzag chains of $(C_2H_5)_3NH^+$ and H_2O. A pair $(C_2H_5)_3NH^+$ column separates two zigzag chains along the *c* axis. There are hydrogen bonds between the N of the ammonium and the O on the bridged oxalate: N1–H1···O5 2.10 Å/146.9°, N1–H1···O8 2.44 Å/131.7°. There are hydrogen bonds between the N of the ammonium and the O on the terminal oxalate: N2–H2···O3 2.20 Å/139°, N2–H2···O4 2.21 Å/143.1°. There are hydrogen bonds between H_2O and the terminal oxalate: O9–H4···O3 2.11 Å/159°, O9–H3···O4 2.20 Å/164°. There are hydrogen bonds between ammonium and H_2O: C8–H8C···O1 2.45 Å/174°; C15–H15A···O8 2.40 Å/155°. The hydrogen bond forms a two-dimensional (2D) network on the (201) plane (Figure 7). There is no hydrogen bond between the one-dimensional $[Cu(\mu\text{-}C_2O_4)(C_2O_4)^{2-})]_n$ chains.

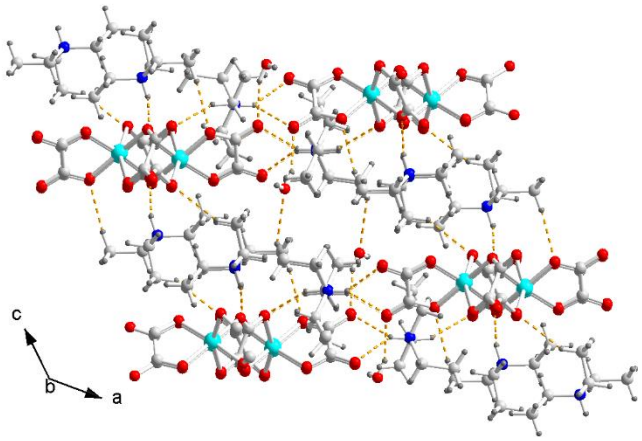

Figure 7. Arrangement of $(C_2H_5)_3NH^+$, zigzag $[Cu(\mu\text{-}C_2O_4)(C_2O_4)^{2-}]_n$ chain and H_2O on two-dimensional hydrogen-bond network viewed along the *b* axis in II. Dashed yellow lines are hydrogen bonds. Color code: Cu, cyan; O, red; C, white; N, blue; H, light grey.

On the basis of the hydrogen bonded cation layer, the resistance, as the proton conductivity under different relative humidities (RH), was measured. Depending on the thermal dynamic analysis, **I** and **II** dehydrate at 40 °C (**I**) and 76 °C (**II**), losing H_2O, with a relative weight of 11.2% in **I** and 4% in **II**; therefore, the experiment should be carried out below 40 °C (Figure 8). When the RH increased, the conductivity of **I** and **II** increased. Under a relatively high RH, the surfaces of the crystal were covered with debris at first, which was solvable in gel. Although the sample was restored to a solid state when the RH decreased and reached the same value as the beginning, the sample turned out to be in a polycrystalline state but not a single crystal. When a single crystal of **I** or **II** was exposed to air under a low relative humidity, such as when the relative humidity was lower than 35%, guest molecules, such as H_2O, in **I** and **II** would escape from the crystal, leading to crystalline collapse. The crystal surface remained transparent and clear after measurements at 20 °C and an RH of 40%. The resistance comes from the intrinsic behavior of the crystal. The resistance is 1×10^9 Ω·cm in **I** and 1×10^7 Ω·cm in **II**. They are insulators.

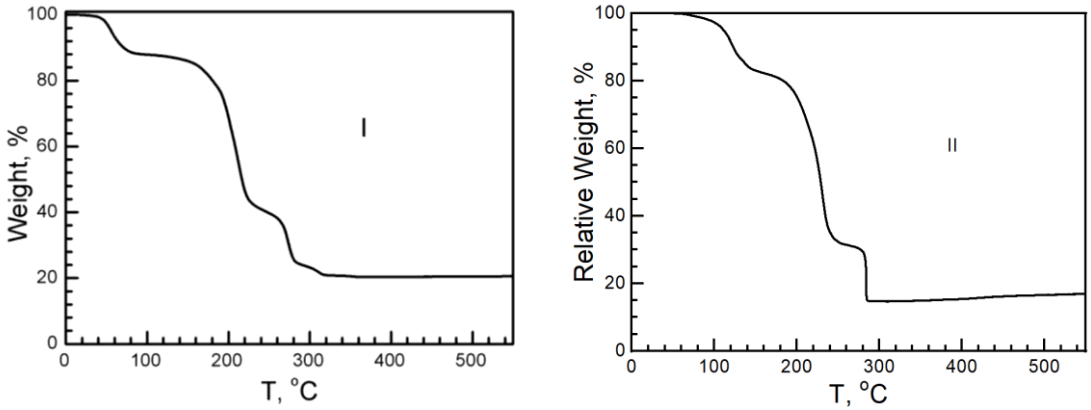

Figure 8. Schematic TGA curves of **I** and **II**. Above 300 °C, the final residue is CuO.

On the basis of the oxalate-bridging and Jahn–Teller distortion of the Cu(II) ion, Cu(II) in an independent unit, and the magnetic properties were studied per Cu^{2+}/mol.

At 300 K, the χT value of **I** was 0.473 cm^3 K mol^{-1} and g = 2.25. It is higher than 0.375 cm^3 K mol^{-1} for an isolated, spin only Cu(II) ion with S = 1/2, g = 2.00 and in the range of Cu^{2+} compounds [34–37,45,46]. The χT value remained stable at 0.478 cm^3 K mol^{-1} at 40 K and increased slowly, reaching 0.71 cm^3 K mol^{-1} at 2 K. No bifurcation is observed from zero-field-cool magnetization and field-cooled magnetization (ZFCM/FCM)

measurements from 2 K to 100 K under 100 G (Figure S4). The magnetic data were fitted with the Curie–Weiss law from 2 to 300 K: C = 0.4711(2) cm^{-1}·K/mol, θ = 0.61(6) K and R = 1.37 × 10^{-5}. It suggests a ferromagnetic interaction in **I** (Figure 9) [47,48].

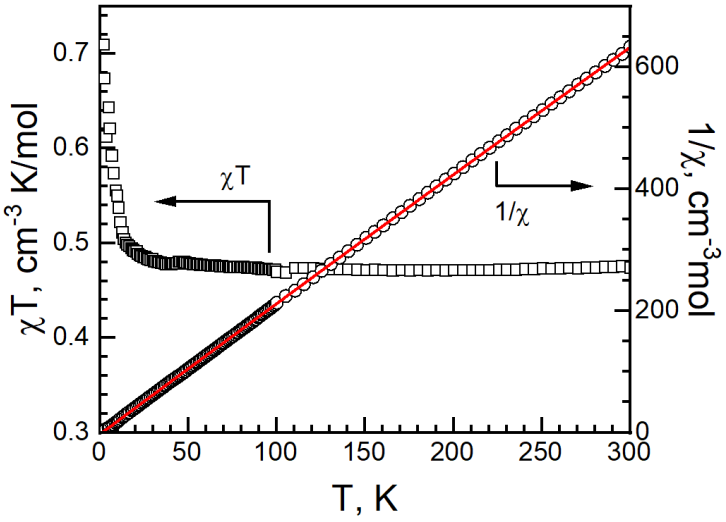

Figure 9. χT vs. T (left, black empty square), $1/\chi$ vs. T (right, black empty circle) and Curie–Weiss fitting data (red solid) of **I**.

A one-dimensional Baker–Rushbrooke–Gilbert model was used to fit the temperature-dependent magnetization above 2 K, yielding J = 0.60(2) cm^{-1}, g = 2.31(1) and R = 9.2 × 10^{-4} (Figure 10) [49]. It shows an intrachain ferromagnetic interaction and corresponds with the Curie–Weiss fitting.

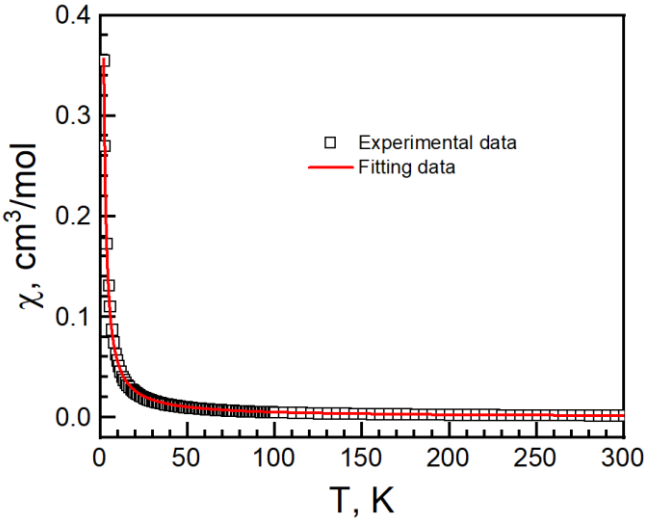

Figure 10. Temperature-dependent susceptibility of **I**. Black empty square is experimental data. Red solid curve is the best fit from the Baker–Rushbrooke–Gilbert model.

At 2 K, the isothermal magnetization (M) saturated at 1.11 Nβ (N is Avogadro's number and β is the Bohn magneton, 1 Nβ = 5585 cm^{-1} G mol^{-1}) at 65 kG (Figure 11). The average anisotropic g-factor calculated from isothermal magnetization at 2 K is 2.22. It is in the range of 2.25 from χT at 300 K and 2.31 from Baker–Rushbrooke–Gilbert model fitting.

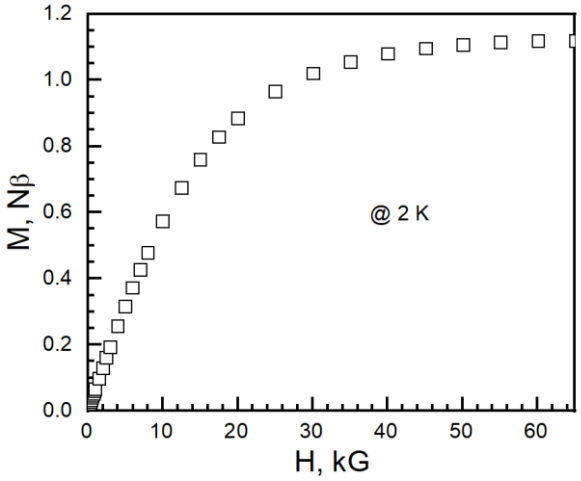

Figure 11. Isothermal magnetization of **I** at 2 K.

In **II**, the χT value was 0.443 cm^3 K mol^{-1} at 300 K with a g-factor of 2.13. It is higher than the 0.375 cm^3 K mol^{-1} of an isolated, spin only Cu(II) ion with $S = 1/2$, $g = 2.00$. It is in the range of Cu^{2+} compounds, as in **I** [34–37,45,46]. As the temperature decreased, the χT value decreased slowly to 0.393 cm^3 K mol^{-1} around 30 K, and then increased, reaching 0.446 cm^3 K mol^{-1} at 2 K (Figure 12). No bifurcation was observed in the ZFCM/FCM measurement from 2 K to 100 K under 100 G (Figure S5). The magnetic data were fitted with Curie–Weiss law from 80 to 300 K with $C = 0.462(1))$ cm^{-1}·K/mol, $g = -14.2(4)$ K and $R = 3.8 \times 10^{-5}$ (Figure 12).

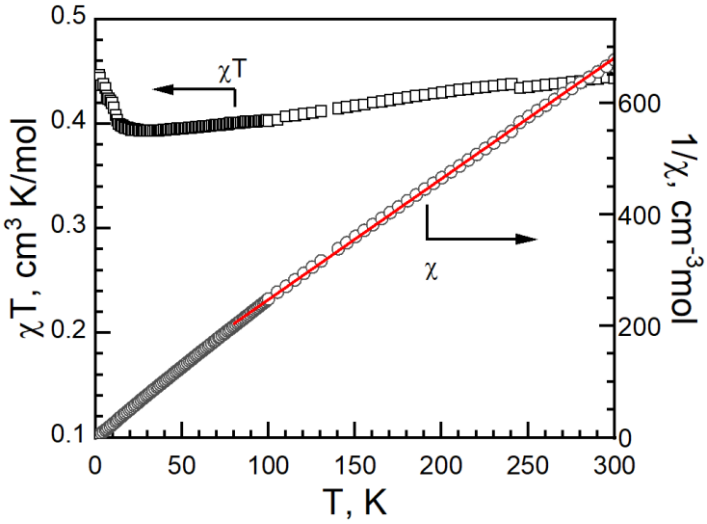

Figure 12. cT vs. T (left, black empty square), $1/c$ vs. T (right, black empty circle) and Curie–Weiss fitting data (red solid) of **II**.

A one-dimensional Baker–Rushbrooke–Gilbert model combined with exchange coupling was used to fit the temperature-dependent magnetization from 2 to 300 K with $J = 0.87(2)$ cm^{-1}, $g = 2.035(3)$, $zJ = -0.65(2)$ cm^{-1} and $R = 6.76 \times 10^{-5}$ (Figure 13) [50]. It shows that intrachain ferromagnetic interaction is stronger than intrachain antiferromagnetic interaction. The g-factor is in the range of 2.13 from χT at 300 K.

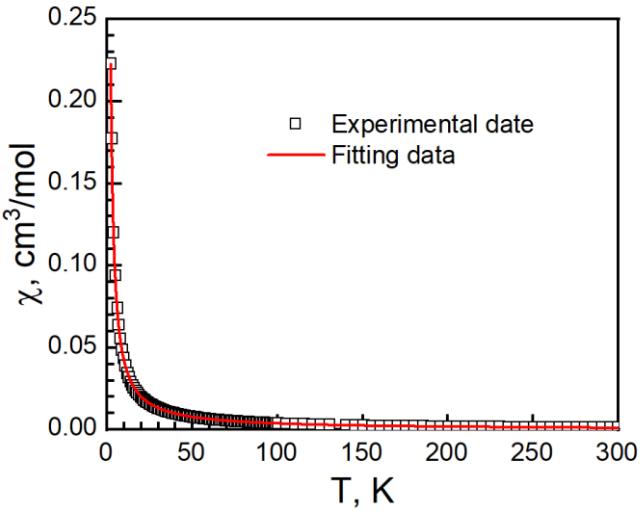

Figure 13. Temperature-dependent susceptibility of **II**. Empty solid square (c), is experimental data. Red solid curve is best fit from the Baker–Rushbrooke–Gilbert model with exchange coupling.

At 2 K, the magnetization increases with increasing field and is saturated at 0.89 Nβ at 65 kG (Figure 14). The average anisotropic *g*-factor calculated from isothermal magnetization at 2 K is 1.78. Its magnetic behavior is not the same as expected. This means the Jahn–Teller effect is important to the magnetic property of the copper-oxalate framework. This is different from the compounds $[CrMn(C_2O_4)_3^-]_n$, where in the ferromagnetic order, temperature and isothermal magnetization at 2 K are the same as those taken from ammonium salts to charge-transfer salts [19,51,52]. Depending on the difference in magnetic behaviors between **I** and **II**, the Jahn–Teller effect will help us to obtain molecular-based candidate quantum spin liquid and to look for a new superconductor and colossal magnetoresistance material from copper-oxalate frameworks as cuprate superconductors and colossal magnetoresistance material.

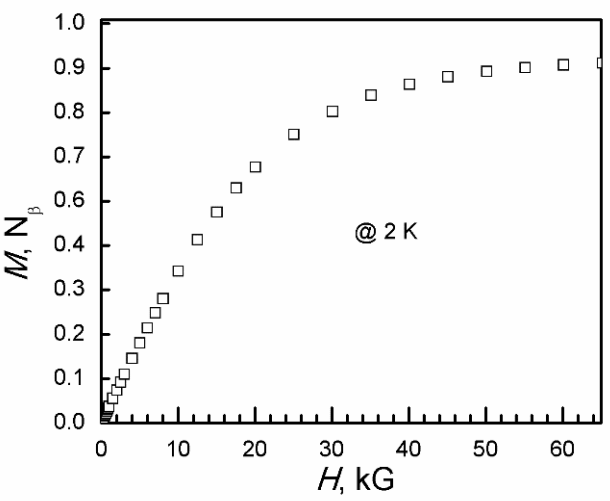

Figure 14. Isothermal magnetization of **II** at 2 K.

4. Conclusions

Two one-dimensional copper-oxalate framework compounds were obtained and characterized. The hydrogen bonds among ammonium, H_2O and the copper-oxalate framework form a three-dimensional hydrogen-bond network, and there is no hydrogen bond between the one-dimensional $[Cu(\mu\text{-}C_2O_4)(C_2O_4)^{2-}]_n$ chains. The Q_3-mode Jahn–Teller distortion of elongated CuO_6 octahedrons is observed. They are insulators. The

Jahn–Teller effect results the ferromagnetic and weak-ferromagnetic interaction between Cu(II) in **I** and **II**. No long-range ordering is observed above 2 K.

Supplementary Materials: Table S1. Crystallographic data of **I** and **II;** Figure S1. IR spectra on crystalline **I** (top) and **II** (bottom); Figure S2. Experimental X-ray powder diffraction pattern of crystalline sample and simulated one based on single crystal structure of **I**. **I** shows preferred orientation; Figure S3. Experimental X-ray powder diffraction pattern of crystalline sample and simulated one based on single crystal structure of **II**; Figure S4. ZFCM/FCM of polycrystal of **I** under 100 G.; Figure S5. ZFCM/FCM of polycrystal of **II** under 100 G.

Author Contributions: The manuscript was written with the contributions of all authors. Funding acquisition: B.Z., D.Z. and Y.Z. Synthesized the sample: Y.Z. Performed the magnetic measurements: Z.W. Performed the single-crystal X-ray diffraction experiments: T.L., Y.S. and M.L. Performed the X-ray experiments and data analysis: B.Z. Conducted experiments: B.Z. and Z.W. Analyzed the data: B.Z., Y.Z. and Z.W. Wrote the main manuscript text. All authors have read and agreed to the published version of the manuscript.

Funding: This research was funded by the National Natural Science Foundation of China: 22273109, 22073106, 21573242 and 21173230 and the Strategic Priority Research Program (B) of the Chinese Academy of Sciences (Grant No. XDB12030100).

Institutional Review Board Statement: Not applicable。

Informed Consent Statement: Not applicable。

Data Availability Statement: The IR spectra, powder X-ray diffraction pattern and ZFCM/FCM of **I** and **II** are available in the Supplementary Materials.

Conflicts of Interest: The authors declare no conflict of interest.

References

1. Jahn, H.A.; Teller, E. Stability of polyatomic molecules in degenerate electronic states-I—Orbital degeneracy. *Proc. R. Soc. Lond. Ser. A Math. Phys. Sci.* **1937**, *161*, 220–235.
2. Opik, U.; Pryce, M.H.L. Studies of the Jahn-Teller effect. I. A survey of the static problem. *Proc. R. Soc. Lond. Ser. A Math. Phys. Sci.* **1957**, *238*, 425–427.
3. Longuet-Higgins, H.C.; Opik, U.; Pryce, H.I.; Sack, R.A. Studies of the Jahn-Teller effect. II. The dynamical problem. *Proc. R. Soc. Lond. Ser. A Math. Phys. Sci.* **1958**, *244*, 1–16.
4. Bednorz, J.G.; Muller, K.A. Possible high Tc superconductivity in the Ba−La−Cu−O system. *Z. Für Phys. B Condens. Matter* **1986**, *64*, 189–193.
5. Radaelli, P.G.; Cox, D.E.; Marezio, M.; Cheong, S.W.; Schiffer, P.E.; Ramirez, A.P. Simultaneous Structural, Magnetic, and Electronic Transitions in La 1−x Cax MnO_3 with x= 0.25 and 0.50. *Phys. Rev. Lett.* **1995**, *75*, 4488–4491.
6. Dagotto, E.; Hotta, T.; Moreo, A. Colossal magnetoresistant materials: The key role of phase separation. *Phys. Rep.* **2001**, *344*, 1–153.
7. Dagotto, E. Complexity in strongly correlated electronic systems. *Science* **2005**, *309*, 257–262.
8. Goodenough, J.B. Jahn-Teller phenomena in solids. *Annu. Rev. Mater. Sci.* **1998**, *28*, 1–27.
9. Bersuker, I.B. *The Jahn-Teller Effect*; Cambridge University Press, Edinburgh Building: Cambridge, UK, 2006.
10. Staub, U.; Scagnoli, V.; Muleders, A.M.; Janousch, M.; Honda, Z.; Tonnerre, J.M. Charge/orbital ordering vs. Jahn-Teller distortion in La0. 5Sr1. 5MnO_4. *Europhys. Lett.* **2006**, *76*, 926–932.
11. Clement, R.; Decurtins, S.; Gruselle, M.; Train, C. Polyfunctional two-(2D) and three-(3D) dimensional oxalate bridged bimetallic magnets. *Mon. Chem.* **2003**, *134*, 117–135.
12. Daze, C.L.F.; Noa, M.A.; Nenwa, J.; Ohrstrom, L. Natural and synthetic metal oxalates–a topology approach. *CrystEngComm* **2019**, *21*, 6156–6164.
13. Hursthouse, M.B.; Light, M.E.; Price, D.J. One-Dimensional Magnetism in Anhydrous Iron and Cobalt Ternary Oxalates with Rare Trigonal-Prismatic Metal Coordination Environment. *Angew. Chem. Int. Ed.* **2004**, *43*, 472–475.
14. Zhang, B.; Zhang, Y.; Chang, G.; Wang, Z.; Zhu, D. Crystal-to-Crystal Transformation from K_2 [Co $(C_2O_4)_2(H_2O)_2]\cdot 4H_2O$ to K_2 [Co $(\mu\text{-}C_2O_4)(C_2O_4)$]. *Magnetochemistry* **2021**, *7*, 77.
15. Duan, Z.; Zhang, Y.; Zhang, B.; Zhu, D. Co$(C_2O_4)(HO(CH_2)_3OH)$: An antiferromagnetic neutral zigzag chain compound showing long-range ordering of spin canting. *Inorg. Chem.* **2008**, *47*, 9152–9154.
16. Zhang, B.; Wang, Z.; Fujiwara, H.; Kabayashi, H.; Kurmoo, M.; Inoue, K.; Mori, T.; Gao, S.; Zhang, Y.; Zhu, D. Tetrathiafulvalene [FeIII $(C_2O_4)Cl_2$]: An Organic–Inorganic Hybrid Exhibiting Canted Antiferromagnetism. *Adv. Mater.* **2005**, *17*, 1988–1991.

17. Zhang, B.; Wang, Z.; Zhang, Y.; Takahashi, K.; Okano, Y.; Cui, H.; Kobayashi, H.; Inoue, K.; Kurmoo, M.; Pratt, F.; et al. Hybrid Organic—Inorganic Conductor with a Magnetic Chain Anion: κ-$BETS_2$ [$Fe^{III}(C_2O_4)Cl_2$][BETS = Bis (ethylenedithio) tetraselenafulvalene]. *Inorg. Chem.* **2006**, *45*, 3275–3280.
18. Tamaki, H.; Zhong, Z.J.; Matsumoto, N.; Kida, S.; Koikawa, M.; Achiwa, N.; Hashimoto, Y.; Okawa, H. Design of metal-complex magnets. Syntheses and magnetic properties of mixed-metal assemblies {NBu4 [MCr (ox) 3]} x ($NBu4^+$ = tetra (n-butyl) ammonium ion; ox^{2-} = oxalate ion; M = Mn^{2+}, Fe^{2+}, Co^{2+}, Ni^{2+}, Cu^{2+}, Zn^{2+}). *J. Am. Chem. Soc.* **1992**, *114*, 6974–6979.
19. Mathoniere, C.; Nuttall, C.J.; Carling, S.G.; Day, P. Ferrimagnetic mixed-valency and mixed-metal tris (oxalato) iron (III) compounds: Synthesis, structure, and magnetism. *Inorg. Chem.* **1996**, *35*, 1201–1206.
20. Duan, Z.; Zhang, Y.; Zhang, B.; Zhu, D. Two Homometallic Antiferromagnets Based on Oxalato-Bridged Honeycomb Assemblies:$(A)^2[M^{II}(C_2O_4)_3]$(A= Ammonium Salt Derived from Diethylenetriamine; M^{II}= Fe^{2+}, Co^{2+}). *Inorg. Chem.* **2009**, *48*, 2140–2146.
21. Rousse, G.; Rodriguez-Carvajal, J. Oxalate-mediated long-range antiferromagnetism order in Fe_2 $(C_2O_4)_3$ $4H_2O$. *Dalton Trans.* **2016**, *45*, 14311–14316.
22. Zhang, B.; Zhang, Y.; Zhang, J.; Li, J.; Zhu, D. A neutral molecular-based layered magnet [Fe $(C_2O_4)(CH_3OH)]_n$ exhibiting magnetic ordering at $T_N \approx$ 23 K. *Dalton Trans.* **2008**, 5037–5040. DOI: 10.1039/b8057756a
23. Decurtins, S.; Schmalle, H.W.; Schneuwly, P.; Esling, J.; Gutlich, P. A concept for the synthesis of 3-dimensional homo- and bimetallic oxalate-bridged networks $[M_2(ox)_3]_n$. Structural, moessbauer, and magnetic studies in the field of molecular-based magnets. *J. Am. Chem. Soc.* **1994**, *116*, 9521–9528.
24. Hernandez-Molina, M.; Lloret, F.; Ruiz-Perez, C.; Julve, M. Weak Ferromagnetism in chiral 3-dimensional oxalato-bridged cobalt (II) compounds. Crystal structure of $[Co(bpy)_3][Co_2(ox)_3]ClO_4$. *Inorg. Chem.* **1998**, *37*, 4131–4135.
25. Coronado, E.; Galan-Mascaros, J.R.; Gomez-Garzia, C.J.; Martinez-Agudo, J.M. Molecule-based magnets formed by bimetallic three-dimensional oxalate networks and chiral tris (bipyridyl) complex cations. The series $[Z^{II}$ $(bpy)_3][ClO_4][M^{II}Cr^{III}$ $(ox)_3]$(Z^{II}= Ru, Fe, Co, and Ni; M^{II}= Mn, Fe, Co, Ni, Cu, and Zn; ox= oxalate dianion). *Inorg. Chem.* **2001**, *40*, 113–120.
26. Zhang, B.; Zhang, Y.; Zhang, J.; Hao, X.; Zhu, D. Mn $(C_2O_4)(H_2O)_{0.25}$: An antiferromagnetic oxalato-based cage compound. *Dalton Trans.* **2011**, *40*, 5430–5432.
27. Mon, M.; Grancha, T.; Verdaguer, M.; Train, C.; Armentano, D.; Pardo, E. Solvent-Dependent Self-Assembly of an Oxalato-Based Three-Dimensional Magnet Exhibiting a Novel Architecture. *Inorg. Chem.* **2016**, *55*, 6845–6847.
28. Thorarinsdottir, A.E.; Harris, T.D. Metal–organic framework magnets. *Chem. Rev.* **2020**, *120*, 8716–8789.
29. Coronado, E.; Galan-Mascaros, J.R.; Marti-Gastaldo, C. Single chain magnets based on the oxalate ligand. *J. Am. Chem. Soc.* **2008**, *130*, 14987–14989.
30. Anderson, P.W. Resonating valence bonds: A new kind of insulator? *Mater. Res. Bull.* **1973**, *8*, 153–160.
31. Anderson, P.W. The resonating valence bond state in La_2CuO_4 and superconductivity. *Science* **1987**, *235*, 1196–1198.
32. Ramirez, A.P. Strongly geometrically frustrated magnets. *Annu. Rev. Mater. Sci.* **1994**, *24*, 453–480.
33. Balent, I. Spin liquids in frustrated magnets. *Nature* **2010**, *464*, 199–208.
34. Zhang, B.; Zhang, Y.; Zhu, D. $(BEDT\text{-}TTF)_3Cu_2(C_2O_4)_3(CH_3OH)_2$: An organic–inorganic hybrid antiferromagnetic semiconductor. *Chem. Commun.* **2012**, *48*, 197–198.
35. Zhang, B.; Zhang, Y.; Wang, Z.; Gao, S.; Guo, Y.; Liu, F.; Zhu, D. $BETS_3[Cu_2(C_2O_4)_3](CH_3OH)_2$: An organic–inorganic hybrid antiferromagnetic metal (BETS = bisethylene(tetraselenfulvalene)). *CrystEngComm* **2013**, *15*, 3529–3535.
36. Zhang, B.; Zhang, Y.; Wang, Z.; Wang, D.; Yang, D.; Gao, Z.; Chang, G.; Guo, Y.; Mori, T.; Zhao, Z.; et al. Organic–inorganic hybrid metallic conductors based on bis (ethylenedithio) tetrathiafulvalene cations and antiferromagnetic oxalate-bridged copper (ii) dinuclear anions. *J. Mater. Chem. C* **2022**, *10*, 2845–2852.
37. Zhang, B.; Zhang, Y.; Wang, Z.; Wang, D.; Baker, P.; Pratt, F.; Zhu, D. Candidate quantum spin liquid due to dimensional reduction of a two-dimensional honeycomb lattice. *Sci. Rep*. **2014**, *4*, 6451.
38. Zhang, B.; Zhang, Y.; Zhu, D. $[(C_2H_5)_3NH]_2Cu_2(C_2O_4)_3$: A three-dimensional metal–oxalato framework showing structurally related dielectric and magnetic transitions at around 165 K. *Dalton Trans.* **2012**, *14*, 8509–8511.
39. Zhang, B.; Baker, P.; Zhang, Y.; Wang, D.; Wang, Z.; Su, S.; Zhu, D.; Pratt, F.L. Quantum spin liquid from a three-dimensional copper-oxalate framework. *J. Am. Chem. Soc.* **2018**, *140*, 122–125.
40. Sheldrick, G.M. *Shelx-97*, 1997. University of Göttingen, Göttingen.
41. Bain, A.B.; Berry, J.F. Diamagnetic corrections and Pascal's constants. *J. Chem. Educ.* **2008**, *85*, 532–536.
42. Zhang, B. CCDC843075. Available online: http://www.ccdc.cam.ac.uk (access on 5 September 2011).
43. Vilela, R.S.; Oliveira, T.I.; Martins, F.T.; Ellena, J.A.; Lloret, F.; Julve, M.; Cangussu, D. Synthesis, crystal structure and magnetic properties of the helical oxalate-bridged copper(II) chain $\{[(CH_3)_4N]_2[Cu(C_2O_4)_2]\cdot H_2O\}_n$. *Comptes Rendus Chim.* **2012**, *15*, 856–865.
44. Cano, J.; Alemany, P.; Alvarez, M.; Verdaguer, M.; Ruiz, E. Exchange Coupling in Oxalato-Bridged Copper (ii) Binuclear Compounds: A Density Functional Study. *Chem. A Eur. J.* **1998**, *4*, 476–484.
45. Carlin, R.; van Duyneveldt, A. *Magnetic Properties of Transition Metal Compounds*; Springer: New York, NY, USA, 1977; p. 69.
46. Zhang, B.; Zhang, Y.; Zhang, J.; Yan, X.; Zhu, D. Step by step crystal-to-crystal transformation from 1D $K_2Cu(C_2O_4)_2(H_2O)_4$ (1) to 1D $K_2Cu(C_2O_4)_2(H_2O)_2$ (2) and then 1D $K_2Cu(C_2O_4)_2$ (3) by dehydration. *CrystEngComm* **2016**, *18*, 5062–5065.
47. Kahn, O. *Molecular Magnetism*; VCH Publisher Inc.: New York, NY, USA, 1993; pp. 10–29.

48. Mugiraneza, S.; Hallas, A.M. Tutorial: A beginner's guide to interpreting magnetic susceptibility data with the Curie-Weiss law. *Commun. Phys.* **2022**, *5*, 95.
49. Baker, G.A.; Rushbrooke, G.S.; Gilbert, H.E. High-temperature series expansions for the spin-½ Heisenberg model by the method of irreducible representations of the symmetric group. *Phys. Rev.* **1964**, *135*, A1272–A1277.
50. Carling, R.L. *Magnetochemistry*; Springer: Berlin/Heidelberg, Germany, 1986; pp. 132–133.
51. Coronado, E.; Galan-Mascaros, J.R.; Gomez-Gracia, C.J.; Laukhin, V. Coexistence of ferromagnetism and metallic conductivity in a molecule-based layered compound. *Nature* **2000**, *408*, 447–449.
52. Alberola, A.; Coronado, E.; Galan-Mascaros, J.R.; Gimenez-Saiz, C.; Gomez-Garcia, C.J. A molecular metal ferromagnet from the organic donor bis (ethylenedithio) tetraselenafulvalene and bimetallic oxalate complexes. *J. Am. Chem. Soc.* **2003**, *125*, 10774–10775.